Emission lines of Fe XI in the 257–407 Å wavelength region observed in solar spectra from EIS/*Hinode* and SERTS

F. P. Keenan,[1]* R. O. Milligan,[2] D. B. Jess,[1] K. M. Aggarwal,[1] M. Mathioudakis,[1] R. J. Thomas,[2] J. W. Brosius[2,3] and J. M. Davila[2]

[1]*Astrophysics Research Centre, School of Mathematics and Physics, Queen's University, Belfast BT7 1NN*
[2]*Laboratory for Solar Physics, Code 671, Heliophysics Science Division, NASA Goddard Space Flight Center, Greenbelt, MD 20771, USA*
[3]*Department of Physics, The Catholic University of America, Washington, DC 20064, USA*

ABSTRACT

Theoretical emission-line ratios involving Fe XI transitions in the 257–407 Å wavelength range are derived using fully relativistic calculations of radiative rates and electron impact excitation cross-sections. These are subsequently compared with both long wavelength channel Extreme-Ultraviolet Imaging Spectrometer (EIS) spectra from the *Hinode* satellite (covering 245–291 Å) and first-order observations ($\sim$235–449 Å) obtained by the Solar Extreme-ultraviolet Research Telescope and Spectrograph (SERTS). The 266.39, 266.60 and 276.36 Å lines of Fe XI are detected in two EIS spectra, confirming earlier identifications of these features, and 276.36 Å is found to provide an electron density (N_e) diagnostic when ratioed against the 257.55 Å transition. Agreement between theory and observation is found to be generally good for the SERTS data sets, with discrepancies normally being due to known line blends, while the 257.55 Å feature is detected for the first time in SERTS spectra. The most useful Fe XI electron density diagnostic is found to be the 308.54/352.67 intensity ratio, which varies by a factor of 8.4 between $N_e = 10^8$ and 10^{11} cm^{-3}, while showing little temperature sensitivity. However, the 349.04/352.67 ratio potentially provides a superior diagnostic, as it involves lines which are closer in wavelength, and varies by a factor of 14.7 between $N_e = 10^8$ and 10^{11} cm^{-3}. Unfortunately, the 349.04 Å line is relatively weak, and also blended with the second-order Fe X 174.52 Å feature, unless the first-order instrument response is enhanced.

Key words: atomic data – Sun: activity – Sun: corona – Sun: UV radiation.

1 INTRODUCTION

Emission lines arising from transitions in sulphur-like Fe XI have been detected in the spectra of a range of astrophysical sources, including the Sun (Dere 1978) and other cool stars (Laming & Drake 1999), as well as active galaxies (Puchnarewicz, Mason & Siemiginowska 1998). The usefulness of these lines as electron density diagnostics for the emitting plasma was first shown by Kastner & Mason (1978), who employed the atomic physics calculations of Mason (1975) to generate theoretical emission-line ratios for this ion. Since then, several authors have calculated atomic data and theoretical line ratios for Fe XI, particularly for applications to solar spectra (see Bhatia, Doschek & Eissner 2002 and references therein).

Most work on the solar spectrum of Fe XI has focused on the $\sim$180–200 Å wavelength range, containing $3s^23p^4$–$3s^23p^33d$ tran-

sitions (see, for example, Keenan et al. 2005). This is understandable, as this wavelength region contains numerous strong Fe XI lines (including the most intense in the solar spectrum), many of which provide good electron density diagnostics. However, the $\sim$257–407 Å region also contains several Fe XI lines, primarily arising from $3s^23p^4$–$3s3p^5$ transitions. In this paper, we use the most recent atomic physics calculations for Fe XI to analyse solar spectra covering this wavelength region. Specifically, we investigate observational data sets from two missions, namely the Extreme-Ultraviolet Imaging Spectrometer (EIS) on board the *Hinode* satellite and the Solar Extreme-ultraviolet Research Telescope and Spectrograph (SERTS) sounding rocket experiments. The EIS long wavelength channel spectral region is 245–291 Å (Culhane et al. 2007), compared to $\sim$235–449 Å for the SERTS first-order bandpass (Neupert et al. 1992), and both have spectral resolutions of about 0.06 Å [full width at half-maximum(FWHM)]. Although SERTS has a larger wavelength coverage, in principle allowing more lines from the same species to be detected, it has a limited dynamic range as most spectra have been recorded on photographic film. By

*E-mail: F.Keenan@qub.ac.uk

Table 1. Fe XI line identifications in the EIS and SERTS spectra.

Wavelength (Å)	Transition	Note
257.55	$3s^23p^4\,^3P_2$–$3s^23p^3(^4S)3d\,^5D_3$	Detected by both EIS and SERTS.
257.77	$3s^23p^4\,^3P_2$–$3s^23p^3(^4S)3d\,^5D_2$	Detected by EIS.
266.39	$3s^23p^4\,^3P_1$–$3s^23p^3(^4S)3d\,^5D_1$	Detected by EIS.
266.60	$3s^23p^4\,^3P_1$–$3s^23p^3(^4S)3d\,^5D_0$	Detected by EIS.
276.36	$3s^23p^4\,^3P_2$–$3s3p^5\,^1P_1$	Detected by EIS.
308.54	$3s^23p^4\,^1D_2$–$3s3p^5\,^1P_1$	Detected by SERTS. Blended with Fe VI (Brosius et al. 1998).
341.11	$3s^23p^4\,^3P_2$–$3s3p^5\,^3P_1$	Detected by SERTS.
349.04	$3s^23p^4\,^3P_1$–$3s3p^5\,^3P_0$	Detected by SERTS. Blended with second-order Fe X 174.52 Å (Thomas & Neupert 1994).
352.67	$3s^23p^4\,^3P_2$–$3s3p^5\,^3P_2$	Detected by SERTS.
356.53	$3s^23p^4\,^3P_1$–$3s3p^5\,^3P_1$	Detected by SERTS.
358.67	$3s^23p^4\,^3P_0$–$3s3p^5\,^3P_1$	Detected by SERTS. Blended with several lines (Young et al. 1998).
369.16	$3s^23p^4\,^3P_1$–$3s3p^5\,^3P_2$	Detected by SERTS.
406.79	$3s^23p^4\,^1D_2$–$3s3p^5\,^3P_2$	Detected by SERTS. Identified in spectrum by Brickhouse et al. (1995).

contrast, EIS spectra are obtained with CCDs, and hence can reliably detect weaker lines. The combination of wavelength coverage and dynamic range provided by SERTS and EIS allows us to undertake a detailed assessment of the Fe XI emission-line spectrum in the 257–407 Å wavelength region.

2 THEORETICAL LINE RATIOS

The model ion adopted for Fe XI has been discussed in detail by Keenan et al. (2005). Briefly, it consisted of the 24 energetically lowest LS states, yielding a total of 48 fine-structure levels. Experimental energy levels, where available, were obtained from Shirai et al. (1990) and Jupén, Isler & Träbert (1993), with the theoretical results of Aggarwal & Keenan (2003a) being used for the remainder. Electron impact rates were taken from Aggarwal & Keenan (2003b), while for Einstein A-coefficients the data of Aggarwal & Keenan (2003a) were employed. Finally, under solar plasma conditions proton impact excitation is only important for transitions within the $3s^23p^4\,^3P$ ground term, and we have used the calculations of Landman (1980) for this atomic process.

Using the model ion outlined above, in conjunction with an updated version of the statistical equilibrium code of Dufton (1977), relative Fe XI emission-line strengths were calculated as a function of both electron temperature (T_e) and density (N_e). Details of the procedures involved and approximations made may be found in Dufton (1977) and Dufton et al. (1978). Given errors in the adopted atomic data of typically ±10 per cent (see the references above), we would expect the theoretical ratios to be accurate to better than ±20 per cent.

3 OBSERVATIONAL DATA

The solar spectra analysed in the present paper are from two instruments, namely the EIS on board the *Hinode* satellite and several SERTS rocket flights. Our EIS data sets are those of an active region and limb area originally presented and discussed by Brown et al. (2008), to which the reader is referred for details of the EIS instrument and the data reduction and flux calibration procedures. These two features, denoted AR1 and Limb by Brown et al., show the strongest Fe XI emission lines of the solar regions considered by these authors. The spectra are from the EIS long wavelength channel and cover 245–291 Å at a resolution of about 55 mÅ (FWHM).

Our SERTS spectra are those of several quiet and active regions, plus an off-limb area, obtained during rocket flights in 1989 (de-

noted SERTS89), 1991 (SERTS91), 1993 (SERTS93) and 1997 (SERTS97). Details of these observations, including their reduction and flux calibration, may be found in Thomas & Neupert (1994) for SERTS89, Brosius et al. (1996) for SERTS91 and SERTS93, and Brosius et al. (2000) for SERTS97. Most of these data sets cover the 235–449 Å (SERTS89) or 231–445 Å (SERTS91 and SERTS93) wavelength regions in first order, at resolutions between 50 and 80 mÅ, with spectra recorded on photographic film. However, the intensity calibrations for the SERTS91 and SERTS93 spectra are highly uncertain for wavelengths shorter than 274 Å. By contrast, the SERTS97 spectrum spans 299–353 Å in first order, at a resolution of 115 mÅ, and was recorded on a CCD. We note that the version of SERTS flown in 1989 carried a standard gold-coated toroidal diffraction grating, while those in 1991, 1993 and 1997 incorporated a multilayered-coated grating which enhanced the instrument sensitivity in the first-order wavelength range, by factors of up to 9. In addition, the absolute intensity calibration of the SERTS89 spectrum has been re-evaluated since the publication of Thomas & Neupert, as a result of which emission-line intensities are uniformly a factor of 1.24 larger than those quoted in that paper (see, for example, Keenan et al. 2008 and references therein).

4 RESULTS AND DISCUSSION

We have searched for Fe XI emission lines in the EIS and SERTS spectra using the detections of Brown et al. (2008) and Thomas & Neupert (1994), supplemented with those from other sources, including the National Institute of Standards and Technology data base,[1] the latest version (V6.0) of the CHIANTI data base (Dere et al. 1997; Dere et al. 2009), and the Atomic Line List of van Hoof.[2] In Table 1, we list the Fe XI transitions identified in the data sets, along with their measured wavelengths. We also provide a note on each line, including whether it is detected in both EIS and SERTS spectra, and if there are possible blending features.

Intensities and linewidths (FWHM) of the Fe XI features are given in Tables 2 and 3–9 for the EIS and SERTS data sets, respectively, along with the associated 1σ errors. In the case of EIS, we have remeasured the spectra considered by Brown et al. (2008) using a standard least-squares fitting routine in SSWIDL assuming Gaussian profiles and a constant background. For SERTS, the measurements were made with modified versions of the Gaussian fitting routines

Table 2. Fe XI line intensities and widths from the EIS spectra.

Feature[a]	Wavelength (Å)	Intensity (erg cm^{-2} s^{-1} sr^{-1})	Linewidth (mÅ)
Active region	257.55	335.0 ± 31.1	73 ± 5
	257.77	167.0 ± 24.2	55 ± 8
	266.39	17.0 ± 3.4	70 ± 4
	266.60	107.0 ± 9.1	90 ± 4
	276.36	16.0 ± 7.7	82 ± 10
Limb	257.55	278 ± 23.9	77 ± 5
	257.77	133.0 ± 14.2	59 ± 9
	266.39	19.0 ± 3.3	96 ± 14
	266.60	45.0 ± 6.8	100 ± 9
	276.36	6.0 ± 2.5	85 ± 10

[a]The active region and limb features are those denoted AR1 and Limb, respectively, by Brown et al. (2008).

Table 3. Fe XI line intensities and widths from the SERTS 1989 active region spectrum (SERTS89–AR).

Wavelength (Å)	Intensity (erg cm^{-2} s^{-1} sr^{-1})	Linewidth (mÅ)
257.55	35.5 ± 15.1	96 ± 10
308.54[a]	106.5 ± 20.3	122 ± 12
341.11	46.1 ± 6.9	93 ± 8
349.04	26.2 ± 11.9	105 ± 39
352.67	161.6 ± 18.8	95 ± 6
356.53	22.1 ± 4.8	92 ± 17
358.67	88.7 ± 11.4	144 ± 9
369.16	47.1 ± 6.3	102 ± 5
406.79	3.6 ± 1.4	57 ± 13

[a]Line measured at wavelength of 308.58 Å in this spectrum (see Section 4.2 for details).

Table 4. Fe XI line intensities and widths from the SERTS 1991 active region spectrum (SERTS91–AR).

Wavelength (Å)	Intensity (erg cm^{-2} s^{-1} sr^{-1})	Linewidth (mÅ)
308.54	5.9 ± 1.7	40 ± 10
341.11	20.3 ± 3.7	56 ± 12
352.67	36.8 ± 5.6	57 ± 7
358.67	19.4 ± 4.9	64 ± 20
369.16	13.4 ± 3.6	69 ± 10

Table 5. Fe XI line intensities and widths from the SERTS 1991 quiet Sun spectrum (SERTS91–QS).

Wavelength (Å)	Intensity (erg cm^{-2} s^{-1} sr^{-1})	Linewidth (mÅ)
308.54	19.2 ± 5.7	38 ± 5
341.11	58.6 ± 10.3	81 ± 14
352.67	112.6 ± 16.1	58 ± 10
356.53	17.2 ± 7.8	45 ± 15
358.67	14.2 ± 8.1	41 ± 16
369.16	44.1 ± 12.3	70 ± 22

Table 6. Fe XI line intensities and widths from the SERTS 1991 off-limb spectrum (SERTS91–OL).

Wavelength (Å)	Intensity (erg cm^{-2} s^{-1} sr^{-1})	Linewidth (mÅ)
308.54	42.8 ± 13.1	43 ± 10
341.11	99.7 ± 15.1	94 ± 12
352.67	240.8 ± 29.1	72 ± 8
358.67	36.3 ± 18.2	37 ± 10
369.16	59.9 ± 8.3	109 ± 30

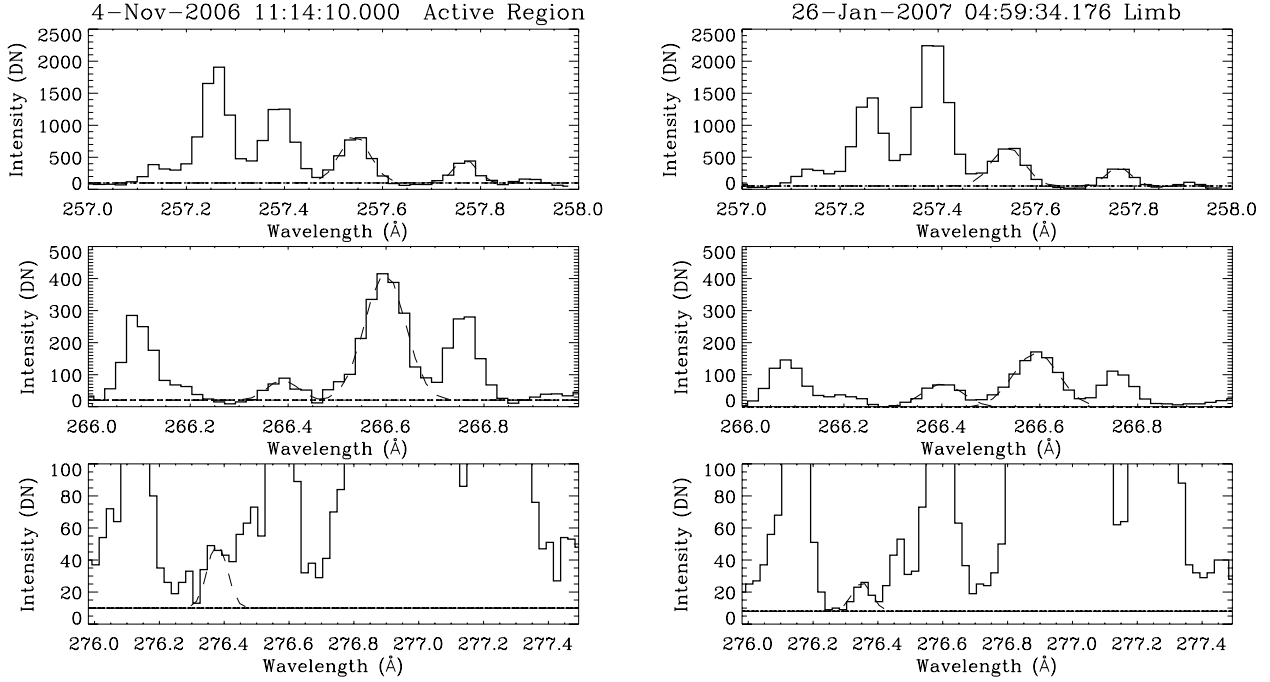**Table 7.** Fe XI line intensities and widths from the SERTS 1993 active region spectrum (SERTS93–AR).

Wavelength (Å)	Intensity (erg cm^{-2} s^{-1} sr^{-1})	Linewidth (mÅ)
308.54	28.7 ± 11.6	45 ± 15
341.11	71.1 ± 10.1	62 ± 9
352.67	178.1 ± 20.5	57 ± 9
356.53	19.3 ± 8.5	42 ± 25
358.67	61.1 ± 11.5	100 ± 17
369.16	59.8 ± 13.4	103 ± 22

Table 8. Fe XI line intensities and widths from the SERTS 1993 quiet Sun spectrum (SERTS93–QS).

Wavelength (Å)	Intensity (erg cm^{-2} s^{-1} sr^{-1})	Linewidth (mÅ)
308.54	6.6 ± 3.2	32 ± 12
341.11	13.5 ± 2.8	50 ± 10
352.67	48.3 ± 6.5	63 ± 9
358.67	10.3 ± 2.9	83 ± 16
369.16	13.2 ± 3.4	115 ± 23

Table 9. Fe XI line intensities and widths from the SERTS 1997 active region spectrum (SERTS97–AR).

Wavelength (Å)	Intensity (erg cm^{-2} s^{-1} sr^{-1})	Linewidth (mÅ)
308.54	33.9 ± 9.8	142 ± 8
341.11	37.8 ± 6.7	149 ± 9
349.04	12.5 ± 4.2	103 ± 9
352.67	136.1 ± 22.1	135 ± 9

originally employed by Thomas & Neupert (1994), as discussed by Keenan et al. (2007). As a consequence, the EIS and SERTS line intensities, FWHM values and their errors listed in Tables 2–9 are somewhat different from those originally reported in Brown et al., Thomas & Neupert and Brosius et al. (1996, 2000). However, in most directly comparable cases, the measured intensity and width values usually differ only slightly from those previously obtained. An exception is the 349.04 Å line in the SERTS spectra, where the features around 349 Å have been fitted with a triple Gaussian as opposed to the double Gaussian adopted by Thomas & Neupert and Brosius et al. This was to allow for the presence of the weak Fe x 349.30 Å transition, instead of only Mg VI 349.16 Å.

Figure 1. Portions of the EIS active region and limb spectra containing the Fe XI 257.55, 257.77, 266.39, 266.60 and 276.36 Å emission lines. The profile fits to these features are shown by dashed lines.

4.1 EIS spectra

Although CHIANTI lists 23 transitions of Fe XI in the EIS long wavelength channel (245–291 Å), most of these are either too weak to be detected or blended with much stronger emission features from other species. As a result, we only have measurements for five lines, which are summarized in Table 2. Portions of the EIS active region and limb spectra containing these lines are shown in Fig. 1. In Table 10, we list the resultant observed line ratios (and their 1σ errors), along with the theoretical results from the present calculations. Also given are the theoretical predictions from the CHIANTI V6.0 data base, which employs the electron excitation rates of Gupta & Tayal (1999) and Bhatia & Doschek (1996). The 266.39/257.55 and 266.60/257.55 ratios are relatively insensitive to changes in the electron density over the range $N_e = 10^9$–10^{11} cm^{-3}, varying by only 13 and 8 per cent, respectively. However, 276.36/257.55 is N_e-sensitive, as may be seen in Fig. 2. Hence, we have determined values of N_e for the active region and limb using the 200.03/202.04 and 203.17/202.04 line intensity ratios in Fe XIII, which is formed at a similar temperature to Fe XI in ionization equi-

Table 10. Fe XI line ratios from the EIS spectra.

Feature	Line ratio	Observed	Present theory[a]	CHIANTI theory[a]
Active region	257.77/257.55	0.50 ± 0.09	0.62	0.52
Active region	266.39/257.55	0.051 ± 0.011	0.12	0.083
Active region	266.60/257.55	0.32 ± 0.04	0.11	0.069
Active region	276.36/257.55	0.048 ± 0.024	0.032	0.038
Limb	257.77/257.55	0.48 ± 0.07	0.61	0.54
Limb	266.39/257.55	0.068 ± 0.013	0.12	0.084
Limb	266.60/257.55	0.16 ± 0.03	0.11	0.072
Limb	276.36/257.55	0.022 ± 0.009	0.041	0.051

[a]Present theoretical ratios and those from CHIANTI calculated at $T_e = 10^{6.1}$ K and $N_e = 10^{9.2}$ cm^{-3} (active region) or $N_e = 10^{9.5}$ cm^{-3} (limb).
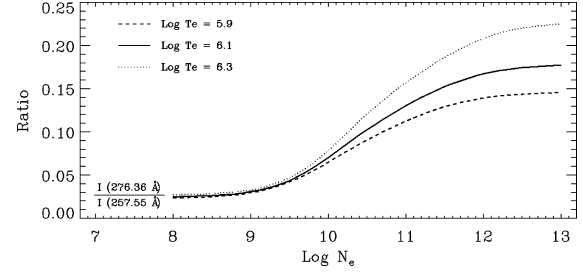
Figure 2. The theoretical Fe XI emission-line intensity ratio I(276.36 Å)/I(257.55 Å), where I is in energy units, plotted as a function of logarithmic electron density (N_e in cm^{-3}) at the temperature of maximum Fe XI fractional abundance in ionization equilibrium, $T_e = 10^{6.1}$ K (Bryans et al. 2009), plus ± 0.2 dex about this value.

librium ($T_e = 10^{6.2}$ K compared to $10^{6.1}$ K for Fe XI; Bryans, Landi & Savin 2009). For the active region, we measured 200.03/202.04 = 0.31 and 203.17/202.04 = 0.16, both of which yield $N_e = 10^{9.2}$ cm^{-3} from the calculations of Keenan et al. (2007). Similarly, for the limb spectrum the observed ratios are 200.03/202.04 = 0.47 and 203.17/202.04 = 0.24, which both indicate $N_e = 10^{9.5}$ cm^{-3}. In Table 10, we therefore list the theoretical ratios generated at the temperature of maximum Fe XI fractional abundance in ionization equilibrium and at densities of $10^{9.2}$ and $10^{9.5}$ cm^{-3} for the active region and limb area, respectively.

The 266.39 Å line was tentatively identified by Träbert (1998) in the solar flare spectra of Dere (1978), and the reasonable agreement between theory and observation for the 266.39/257.55 ratio in Table 10 (especially for the CHIANTI calculations) supports this identification. We note that CHIANTI lists the $3s^23p^4\,^3P_1$–$3s^23p^3(^4S)3d\,^5D_1$ transition at 273.41 Å, but no emission feature is detected at this wavelength in the EIS spectra. In addition, Brown et al. (2008) identify the 266.39 Å feature as an Fe XVII transition. However, the fact that the measured 266.39/257.55 ratios are actually somewhat

smaller than theory indicates that Fe XVII probably makes a negligible contribution to the 266.39 Å line intensity.

Träbert (1998) also tentatively identified the 266.60 Å line of Fe XI in the Dere (1978) spectra, but in this case the experimental 266.60/257.55 ratios in Table 10 are larger than the theoretical values, at least for the active region. This suggests that the 266.60 Å feature is blended, which is supported by the relatively large width found for the line. However, an inspection of CHIANTI and other line lists reveals no likely blending candidates. We note that CHIANTI lists a wavelength of 273.57 Å for the $3s^2 3p^4\,^3P_1$–$3s^2 3p^3(^4S)3d\,^5D_0$ transition, which unfortunately would be blended with Fe XIV 273.55 Å. However, the experimental Fe XIV 273.55/274.20 ratios in the EIS spectra are in good agreement with the CHIANTI predictions, indicating that Fe XI does not make a contribution to the 273.55 Å line intensity. We also note that Brown et al. (2008) detect the 266.60 Å line, but no identification is provided.

Of particular interest is the 276.36 Å line, which was unidentified in solar observations until recently detected by Brown et al. (2008) in the EIS limb spectrum. However, these authors identify the feature as Fe XII rather than Fe XI, although this is almost certainly a typographical error as the transition is correctly given as $3s^2 3p^4\,^3P_2$–$3s3p^5\,^1P_1$. (We note in passing that Brown et al. incorrectly list the 257.77 Å line as having a $^5D_4$ upper level, when it should be $^5D_2$.) An inspection of Table 10 reveals good agreement between theory and observation for 276.36/257.55, confirming the identification of the 276.36 Å feature as the $3s^2 3p^4\,^3P_2$–$3s3p^5\,^1P_1$ line of Fe XI. However, further observations of the transition would be useful, as the 276.36/257.55 ratio potentially provides a useful EIS long wavelength channel density diagnostic for the Fe XI–emitting region of a plasma, as it varies by a factor of 6.8 between $N_e = 10^8$ and $10^{12}\,cm^{-3}$.

In Table 10, we also list the observed and theoretical 257.77/257.55 ratios, for which there is good agreement, indicating that both lines are well resolved in the EIS spectra and free from blends. To check this, we have generated synthetic active region, flare and quiet Sun spectra using V6.0 of the CHIANTI data base. These reveal no significant blends for either the 257.55 or 257.77 Å transitions, nor indeed for the 276.36 Å feature. We note that Jupén et al. (1993) originally identified the 257.55 and 257.77 Å features as being the (2–3) and (2–2) components, respectively, of the $3s^2 3p^4\,^3P_J$–$3s^2 3p^3(^4S)3d\,^5D_{J'}$ multiplet. Subsequently, Träbert (1998) reclassified the lines as the (2–2) and (2–1) components, with (2–3) lying at 257.26 Å and hence blended with a strong Fe X line. However, the theoretical (2–1)/(2–2) ratio is 0.31 (present calculations) or 0.27 (CHIANTI), much smaller than the experimental values of around 0.50 for 257.77/257.55. Hence, the EIS observations do not support the Träbert classifications, but rather those of Jupén et al. A definitive answer would be provided by the unambiguous detection of the (1–2) or (2–1) components of the multiplet. Unfortunately, the (1–2) transition is predicted to be too weak to observe, with a theoretical intensity of less than 0.1 per cent that of the 257.55 Å feature. Similarly, the (2–1) transition is predicted to lie at 264.92 Å by CHIANTI, and cannot be observed as it lies between lines of Fe XIV and Fe XVI.

4.2 SERTS observations

The SERTS first-order wavelength range (~ 235–449 Å) contains numerous Fe XI emission features, resulting in many possible line ratio combinations. Following Keenan et al. (2007), we categorize three types of ratio, namely

Table 11. Comparison of theory and observation for SERTS line ratios involving transitions from common upper levels.

Feature	Line ratio	Observed	Present theory	CHIANTI theory
SERTS89–AR	341.11/356.53	2.1 ± 0.6	2.0	2.0
SERTS91–QS	341.11/356.53	3.4 ± 1.7	2.0	2.0
SERTS93–AR	341.11/356.53	3.7 ± 1.7	2.0	2.0
SERTS89–AR	341.11/358.67	0.52 ± 0.10	1.6	1.6
SERTS91–AR	341.11/358.67	1.0 ± 0.3	1.6	1.6
SERTS93–QS	341.11/358.67	1.3 ± 0.5	1.6	1.6
SERTS89–AR	358.67/356.53	4.0 ± 1.0	1.2	1.3
SERTS91–QS	358.67/356.53	0.83 ± 0.60	1.2	1.3
SERTS93–AR	358.67/356.53	3.2 ± 1.5	1.2	1.3
SERTS89–AR	369.16/352.67	0.29 ± 0.05	0.30	0.30
SERTS91–AR	369.16/352.67	0.36 ± 0.11	0.30	0.30
SERTS91–QS	369.16/352.67	0.39 ± 0.12	0.30	0.30
SERTS91–OL	369.16/352.67	0.25 ± 0.05	0.30	0.30
SERTS93–AR	369.16/352.67	0.34 ± 0.09	0.30	0.30
SERTS93–QS	369.16/352.67	0.27 ± 0.08	0.30	0.30
SERTS89–AR	406.79/352.67	0.022 ± 0.009	0.023	0.027

(i) branching ratios, where the transitions arise from a common upper level. In this instance, the ratio is predicted to be constant under most plasma conditions, an exception being when significant opacity is present, which should not apply to the Fe XI lines considered here;

(ii) ratios which are predicted to be relatively insensitive to changes in T_e and N_e over the range of plasma parameters of interest;

(iii) ratios which are predicted to vary significantly with N_e, and hence may provide useful electron density diagnostics.

Ratios in categories (i) and (ii) are the most useful for identifying and assessing the importance of blends, as well as investigating possible errors in the adopted atomic data, as one does not need to accurately know the plasma parameters to generate a theoretical ratio for comparison with observations. In Tables 11 and 12, we therefore list the observed line ratios for the SERTS data sets which fall into category (i) and (ii), respectively (along with the associated 1σ errors), as well as the theoretical values both from the present calculations and CHIANTI. Once again, following Keenan et al. (2007), we have defined 'relatively insensitive' as being those ratios which are predicted to vary by less than ± 20 per cent when the electron density is changed by a factor of 2 (i.e. ± 0.3 dex). In fact, most of the ratios in Table 12 show much lower sensitivity to variations in N_e. For example, at $T_e = 10^{6.1}$ K, the 341.11/352.67 ratio only changes from 0.27 at $N_e = 10^9\,cm^{-3}$ to 0.31 at $N_e = 10^{10}\,cm^{-3}$, while 257.55/352.67 varies from 0.13 to 0.16 over the same density interval. As noted by Keenan et al., most of the electron densities derived for SERTS active regions from species formed at similar temperatures to Fe XI are consistent with log $N_e = 9.4 \pm 0.3$. This is also the case for both quiet Sun regions and the off-limb area, where diagnostics indicate log $N_e = 9.1 \pm 0.3$ (Brosius et al. 1996). The theoretical results in Table 12 have therefore been calculated at the temperature of maximum Fe XI fractional abundance in ionization equilibrium, $T_e = 10^{6.1}$ K (Bryans et al. 2009), and at $N_e = 10^{9.4}\,cm^{-3}$ (for the active regions) or $10^{9.1}\,cm^{-3}$ (quiet Sun and off-limb). However, we note that changing the adopted value of T_e by ± 0.2 dex or the density by ± 0.5 dex does not significantly alter the discussions below.

An inspection of Table 12 reveals good agreement between theory and observation for the 257.55/352.67 ratio, providing support

**Table 12.** Comparison of theory and observation for SERTS line ratios which are only weakly N_e-dependent.

Feature	Line ratio	Observed	Present theory[a]	CHIANTI theory[a]
SERTS89–AR	257.55/352.67	0.22 ± 0.10	0.14	0.19
SERTS89–AR	341.11/352.67	0.29 ± 0.05	0.29	0.28
SERTS91–AR	341.11/352.67	0.55 ± 0.13	0.29	0.28
SERTS91–QS	341.11/352.67	0.52 ± 0.12	0.28	0.27
SERTS91–OL	341.11/352.67	0.41 ± 0.08	0.28	0.27
SERTS93–AR	341.11/352.67	0.40 ± 0.07	0.29	0.28
SERTS93–QS	341.11/352.67	0.28 ± 0.07	0.28	0.27
SERTS97–AR	341.11/352.67	0.28 ± 0.07	0.29	0.28
SERTS89–AR	349.04/308.54	0.25 ± 0.12	0.65	0.50
SERTS97–AR	349.04/308.54	0.37 ± 0.16	0.65	0.50
SERTS89–AR	356.53/352.67	0.14 ± 0.03	0.14	0.14
SERTS91–QS	356.53/352.67	0.15 ± 0.07	0.14	0.13
SERTS93–AR	356.53/352.67	0.11 ± 0.05	0.14	0.14
SERTS89–AR	358.67/352.67	0.55 ± 0.10	0.18	0.18
SERTS91–AR	358.67/352.67	0.53 ± 0.16	0.18	0.18
SERTS91–QS	358.67/352.67	0.13 ± 0.08	0.17	0.17
SERTS91–OL	358.67/352.67	0.15 ± 0.08	0.17	0.17
SERTS93–AR	358.67/352.67	0.34 ± 0.08	0.18	0.18
SERTS93–QS	358.67/352.67	0.21 ± 0.07	0.17	0.17

[a]Present theoretical ratios and those from CHIANTI calculated at $T_e = 10^{6.1}$ K and $N_e = 10^{9.4}$ cm^{-3} (for active regions) or $N_e = 10^{9.1}$ cm^{-3} (quiet Sun and off-limb regions).

for our identification of the 257.55 Å line. This is the first time this feature has been detected in SERTS observations, although it has previously been identified by Jupén et al. (1993) in the solar spectrum of Behring et al. (1976), as well as in EIS data (see Section 4.1).

The measured 349.04/308.54 ratio in Table 12 for the SERTS89 active region is smaller than the present theoretical result or that from CHIANTI, which indicates blending in the 308.54 Å line. Brosius, Davila & Thomas (1998) note that the Fe XI 308.54 Å feature is blended with an Fe VI transition, but from the CHIANTI synthetic spectra the latter is predicted to contribute less than 0.1 per cent of the total intensity. Indeed, CHIANTI indicates that there are lines of Ni XIII, Al VI and Ne III which make a larger contribution to the blend than Fe VI, but even then the summed intensity of these three transitions is only 5 per cent that of Fe XI. On the other hand, the 308.54 Å linewidth in the SERTS89 active region spectrum is much larger than in the other SERTS data sets, as may be seen from Fig. 3 and Tables 3–9. Furthermore, the feature lies at 308.58 Å in the SERTS89 observations, compared to 308.54 Å in the remaining SERTS data sets and other solar spectra, such as those from the S082A instrument on board *Skylab* (Dere 1978). Both the large linewidth and wavelength shift are symptomatic of blending, but if such a species is present it is difficult to explain why it should affect one active region and not others. A more likely explanation is a fault with the SERTS spectrum, although an inspection of the film reveals no apparent flaws.

The experimental 349.04/308.54 ratio for the SERTS97 active region is in good agreement with theory, indicating that both these features are reliably observed and free from blends. Thomas & Neupert (1994) point out that the Fe XI 349.04 Å line in the SERTS89 data is blended with the second-order Fe X 174.52 Å transition, which appears at 349.04 Å in first order. However, as noted in Section 3, the version of SERTS flown in 1997 incorporated a multilayered-coated grating, which enhanced the instrument sensitivity in first order compared to the SERTS89 observations, hence removing the
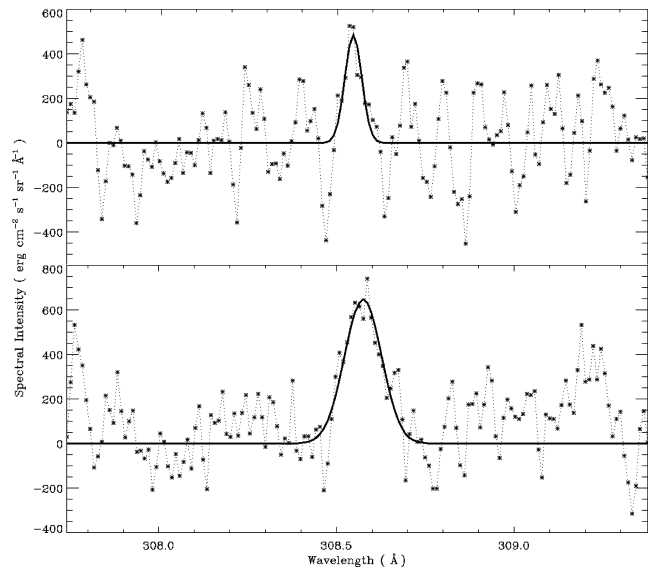
Figure 3. Plot of the SERTS 1989 (lower panel) and 1993 (upper panel) active region spectra in the 307.8–309.3 Å wavelength range. The profile fits to the Fe XI 308.54 Å feature are shown by solid lines.

effect of the blend with Fe X 174.52 Å. On the other hand, this blending is evident in the spectrum from the SERTS flight in 1995, where the instrument sensitivity was enhanced in the second-order waveband (Brosius et al. 1998), and the observed 349.04/308.54 ratio is 3.4, much larger than the theoretical value of about 0.6.

Both the experimental 341.11/356.53 and 341.11/352.67 ratios in Tables 11 and 12 are generally larger than the theoretical values, which CHIANTI indicates is due to blending of 341.11 Å with an Fe IX transition. The latter is predicted to contribute about 33 per cent to the total 341.11 Å line intensity, which is consistent with the observations. For example, for the SERTS93 active region, reducing the intensity of the 341.11 Å line by 33 per cent leads to a revised 341.11/352.67 ratio of 0.26, in good agreement with the theoretical value of 0.29.

The measured 356.53/352.67 ratios in Table 12 are all in good agreement with theory, indicating that both the 352.67 and 356.53 Å lines are well observed and free from blends. Similarly, there are no discrepancies between theory and observation for 369.16/352.67, and indeed the average of the six measurements in Table 11 is 0.32 ± 0.05, which compares very well with the theoretical result of 0.30, showing that the 369.16 Å transition is also free from blends. We note that the 352.67, 356.53 and 369.16 Å lines of Fe XI have also been recently observed by the Extreme-Ultraviolet Normal Incidence Spectrograph solar instrument (Brosius et al. 2008), and show good agreement between theory and experiment, with measured ratios of $356.53/352.67 = 0.16 \pm 0.03$ and $369.16/352.67 = 0.30 \pm 0.05$, compared to the theoretical estimates of 0.14 and 0.30, respectively.

Young, Landi & Thomas (1998) note that the 358.67 Å line of Fe XI is blended with several transitions of Si XI, Ne IV and Fe XIV. However, the observed 358.67/356.53 and 358.67/352.67 ratios in Tables 11 and 12 are only much larger than the theoretical values for the active region spectra, with measurements for the quiet Sun and off-limb regions being in good agreement with theory. This implies that blending of 358.67 Å is only significant in active regions. By contrast, the synthetic active region and quiet Sun spectra generated with CHIANTI predict that Fe XI should make a smaller contribution to the total 358.67 Å line intensity in the latter (less than 20 per cent

compared to about 35 per cent in an active region), and hence that blending of the Fe xi feature should in fact be more severe in quiet Sun spectra. However, Fe xi observations from other solar missions support the present findings. For example, for a quiet solar region observed with the CDS instrument on the *SOHO* satellite, Landi, Feldman & Dere (2002) measured Fe xi ratios of 358.67/356.53 = 1.1 ± 0.1 and 358.67/352.67 = 0.14 ± 0.02, in excellent agreement with the theoretical values of 1.2 and 0.17, respectively. Better agreement between theory and observation for the quiet Sun compared to active regions is indicative of blending with lines formed at higher temperatures than Fe xi. Our results would therefore suggest that Si xi and Fe xiv (both of which are formed at slightly higher temperatures than Fe xi) make a larger contribution to the 358.67 Å line intensity than currently predicted by CHIANTI, while Ne iv makes a smaller contribution.

Finally, the observed 406.79/352.67 ratio in Table 11 is in very good agreement with the present calculations and also those from CHIANTI, supporting the identification of the 406.79 Å line in the SERTS89 active region spectrum by Brickhouse, Raymond & Smith (1995).

4.3 Electron density diagnostics from SERTS spectra

In Figs 4 and 5, we plot the electron density diagnostics 308.54/352.67 and 349.04/352.67, respectively, while in Table 13 we list the observed ratios (and the associated 1σ errors) along with the values of N_e derived using the theoretical results at the temperature of maximum Fe xi fractional abundance in ionization equilibrium, $T_e = 10^{6.1}$ K (Bryans et al. 2009). However, we note that changing T_e by ± 0.2 dex would lead to a variation in the derived values of N_e of at most ± 0.1 dex. Also listed in the table is
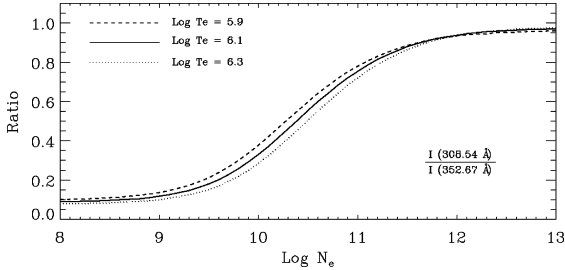
Figure 4. The theoretical Fe xi emission-line intensity ratio I(308.54 Å)/I(352.67 Å), where I is in energy units, plotted as a function of logarithmic electron density (N_e in cm^{-3}) at the temperature of maximum Fe xi fractional abundance in ionization equilibrium, $T_e = 10^{6.1}$ K (Bryans et al. 2009), plus ± 0.2 dex about this value.
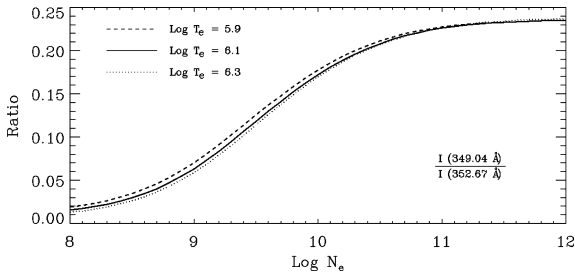
Figure 5. The theoretical Fe xi emission-line intensity ratio I(349.04 Å)/I(352.67 Å), where I is in energy units, plotted as a function of logarithmic electron density (N_e in cm^{-3}) at the temperature of maximum Fe xi fractional abundance in ionization equilibrium, $T_e = 10^{6.1}$ K (Bryans et al. 2009), plus ± 0.2 dex about this value.

Table 13. Electron density diagnostic line ratios from the SERTS spectra.

Feature	Line ratio	Observed	$\log N_e^a$	Ratio variation^b
SERTS89–AR	308.54/352.67	0.66 ± 0.15	$10.7^{+0.5}_{-0.3}$	8.4
SERTS91–AR	308.54/352.67	0.16 ± 0.05	$9.4^{+0.2}_{-0.5}$	8.4
SERTS91–QS	308.54/352.67	0.17 ± 0.06	$9.4^{+0.3}_{-0.5}$	8.4
SERTS91–OL	308.54/352.67	0.18 ± 0.06	$9.5^{+0.2}_{-0.5}$	8.4
SERTS93–AR	308.54/352.67	0.16 ± 0.07	$9.4^{+0.3}_{-1.3}$	8.4
SERTS93–QS	308.54/352.67	0.14 ± 0.07	$9.2^{+0.4}_{-\infty}$	8.4
SERTS97–AR	308.54/352.67	0.25 ± 0.08	$9.8^{+0.2}_{-0.4}$	8.4
SERTS89–AR	349.04/352.67	0.16 ± 0.08	$9.9^{+\infty}_{-0.7}$	14.7
SERTS97–AR	349.04/352.67	0.092 ± 0.034	$9.3^{+0.3}_{-0.4}$	14.7

^{a}Determined from present line ratio calculations at $T_e = 10^{6.1}$ K; N_e in cm^{-3}.
^{b}Factor by which the theoretical line ratio varies between $N_e = 10^8$ and 10^{11} cm^{-3}.

the factor by which the relevant ratio is predicted to vary between $N_e = 10^8$ and 10^{11} cm^{-3}.

An inspection of Table 13 reveals that the densities derived from 308.54/352.67 are generally in very good agreement with those estimated for the SERTS solar features from line ratios in species formed at similar temperatures to Fe xi, which as noted in Section 4.2 average about $\log N_e = 9.4 \pm 0.3$ for active regions and $\log N_e = 9.1 \pm 0.3$ for quiet Sun and off-limb areas. Hence, we can state that, in general, the 308.54/352.67 ratio appears to provide a good N_e diagnostic. The exception is the SERTS89 active region, where the derived density is more than an order of magnitude larger than expected. However, as already discussed in Section 4.2, there are problems with the 308.54 Å feature in the SERTS89 active region observations which make its measurement uncertain.

The electron density derived for the SERTS97 active region from the 349.04/352.67 ratio is in good agreement with those found from other species, but in the case of the SERTS89 active region the density is much higher than expected. However, as noted by Thomas & Neupert (1994), the 349.04 Å line in the SERTS89 observations is blended with the second-order Fe x 174.52 Å feature. We can estimate its contribution using the nearby Fe x 177.24 Å transition, which appears in first order at 354.48 Å. The first-order intensity of this line is 3.6 erg cm^{-2} s^{-1} sr^{-1}, and the 174.52 Å feature is predicted to be a factor of 1.8 stronger (Keenan et al. 2008), yielding an intensity of 6.5 erg cm^{-2} s^{-1} sr^{-1}. This in turn gives a corrected intensity for Fe xi 349.04 Å of 19.7 erg cm^{-2} s^{-1} sr^{-1}, and revised experimental 349.04/352.67 ratio of 0.12. From Fig. 5, this implies $N_e = 10^{9.5}$ cm^{-3}, in good agreement with other diagnostics.

Although the 308.54/352.67 ratio is probably the most useful Fe xi density diagnostic currently available in the 257–407 Å wavelength range, 349.04/352.67 is superior in many respects. The lines are closer together, reducing the effects of possible errors in the instrument intensity calibration, and the ratio varies by a larger factor over the density range $N_e = 10^8$–10^{11} cm^{-3} (14.7 cf. 8.4 for 308.54/352.67). However, the 349.04 Å feature is relatively weak, and is also blended with Fe x 174.52 Å, unless the first-order instrument response is enhanced, as for the SERTS97 observations.

ACKNOWLEDGMENTS

REFERENCES

Aggarwal K. M., Keenan F. P., 2003a, MNRAS, 338, 412

Aggarwal K. M., Keenan F. P., 2003b, A&A, 399, 799

Behring W. E., Cohen L., Feldman U., Doschek G. A., 1976, ApJ, 203, 521

Bhatia A. K., Doschek G. A., 1996, Atomic Data Nuclear Data Tables, 64, 183

Bhatia A. K., Doschek G. A., Eissner W., 2002, Atomic Data Nuclear Data Tables, 82, 211

Brickhouse N. S., Raymond J. C., Smith B. W., 1995, ApJS, 97, 551

Brosius J. W., Davila J. M., Thomas R. J., Monsignori-Fossi B. C., 1996, ApJS, 106, 143

Brosius J. W., Davila J. M., Thomas R. J., 1998, ApJS, 119, 255

Brosius J. W., Thomas R. J., Davila J. M., Landi E., 2000, ApJ, 543, 1016

Brosius J. W., Rabin D. M., Thomas R. J., Landi E., 2008, ApJ, 677, 781

Brown C. M., Feldman U., Seely J. F., Korendyke C. M., Hara H., 2008, ApJS, 176, 511

Bryans P., Landi E., Savin D. W., 2009, ApJ, 691, 1540

Culhane J. L. et al., 2007, Sol. Phys., 243, 19

Dere K. P., 1978, ApJ, 221, 1062

Dere K. P., Landi E., Mason H. E., Monsignori-Fossi B. C., Young P. R., 1997, A&AS, 125, 149

Dere K. P., Landi E., Young P. R., Del Zanna G., Landini M., Mason H. E., 2009, A&A, 498, 915

Dufton P. L., 1977, Comput. Phys. Communications, 13, 25

Dufton P. L., Berrington K. A., Burke P. G., Kingston A. E., 1978, A&A, 62, 111

Gupta G. P., Tayal S. S., 1999, ApJ, 510, 1078

Jupén C., Isler R. C., Träbert E., 1993, MNRAS, 264, 627

Kastner S. O., Mason H. E., 1978, A&A, 67, 119

Keenan F. P., Aggarwal K. M., Ryans R. S. I., Milligan R. O., Bloomfield D. S., Brosius J. W., Davila J. M., Thomas R. J., 2005, ApJ, 624, 428

Keenan F. P., Jess D. B., Aggarwal K. M., Thomas R. J., Brosius J. W., Davila J. M., 2007, MNRAS, 376, 205

Keenan F. P., Jess D. B., Aggarwal K. M., Thomas R. J., Brosius J. W., Davila J. M., 2008, MNRAS, 389, 939

Laming J. M., Drake J. J., 1999, ApJ, 516, 324

Landi E., Feldman U., Dere K. P., 2002, ApJ, 574, 495

Landman D. A., 1980, ApJ, 240, 709

Mason H. E., 1975, MNRAS, 170, 651

Neupert W. M., Epstein G. L., Thomas R. J., Thompson W. T., 1992, Sol. Phys., 137, 87

Puchnarewicz E. M., Mason K. O., Siemiginowska A., 1998, MNRAS, 293, L52

Shirai T., Funatake Y., Mori K., Sugar J., Wiese W. L., Nakai Y., 1990, J. Phys. Chemical Reference Data, 19, 127

Thomas R. J., Neupert W. M., 1994, ApJS, 91, 461

Träbert E., 1998, MNRAS, 297, 399

Young P. R., Landi E., Thomas R. J., 1998, A&A, 329, 291

This paper has been typeset from a TEX/LATEX file prepared by the author.